How to cite: *Angew. Chem. Int. Ed.* **2022,** *61,* e202206682
International Edition: doi.org/10.1002/anie.202206682
German Edition: doi.org/10.1002/ange.202206682

Li Metal Batteries

Non-Flammable Ester Electrolyte with Boosted Stability Against Li for High-Performance Li Metal Batteries

Zhijie Wang[+], Yanyan Wang[+], Baohua Li, James C. Bouwer, Kenneth Davey, Jun Lu,* and Zaiping Guo**

Abstract: In traditional non-flammable electrolytes a trade-off always exists between non-flammability and battery performance. Previous research focused on reducing free solvents and forming anion-derived solid-electrolyte interphase. However, the contribution of solvated anions in boosting the stability of electrolyte has been overlooked. Here, we resolve this via introducing anions into Li^+ solvation sheaths using anions with similar Gutmann donor number (DN) to that of solvents. Taking trimethyl phosphate fire-retardant (DN = 23.0 kcal mol^{-1}) and NO_3^- (DN = 22.2 kcal mol^{-1}) as an example, NO_3^- is readily involved in the Li^+ solvation sheath and reduces the polarity of solvent. This results in boosted stability of electrolyte against Li. The developed non-flammable electrolyte has low viscosity, high ionic conductivity and is low cost. The reversibility of Li-Cu cell was improved to 99.49 % and the lifespan of practical LMBs was extended by > 100 %.

Introduction

Li metal-based batteries (LMBs) are of significant research interest because of use as high energy density power sources, especially in electric vehicles.[1] Due to reported fires caused by LMBs in recent decades,[2] design for safety has become most important, even superior to the pursuit of high energy density. Using solid-state electrolytes is regarded as an ultimate strategy to obviate threats to fire safety, but a practical difficulty has been to solve the high solid-solid interfacial resistance between electrolyte and electrodes.[3] Liquid electrolytes are expected however to dominate in the near future,[4] particularly if problems of flammability are practically addressed.[2d,5] Therefore researchers have looked at salt-concentrated,[6] high-salt-to-solvent ratio,[7] all-fluorinated[8] and ionic liquid[9] electrolytes to maintain safety whilst boosting cycle life of LMBs. However, inherent disadvantages including, high viscosity, low ionic conductivity and present high cost limit practical applications. Additionally, water-in-salt[10] and molecular crowding electrolytes[11] with high safety were developed. However, because of the existence of water, metallic Li and nickel-rich layered cathode material (such as NCM811) cannot be used in these electrolytes, therefore limiting overall energy density of the batteries. Another approach has been to design for non-flammable electrolytes with addition of fire retardants, usually organic phosphates, to general carbonate electrolytes.[12] However a trade-off exists between non-flammability and battery performance.[7a,12] This is because of poor stability of organic phosphates against Li metal,[13] especially given that > 40 % phosphates is required to achieve a zero self-extinguishing time.[14] Improving the stability of the carbonate-phosphate based electrolyte against Li metal is therefore of significant practical value.

The stability of electrolyte against Li metal is significantly dependent on its solvation structure.[15] Solvent molecules exhibit a reduced lowest unoccupied molecular orbital (LUMO) when complexed with Li^+.[16] In the solvation sheaths, polarized solvent molecules induced by the electrostatic field of Li^+ are more susceptible to accepting electrons and decompose on Li metal surface than free solvents,[17] because of increased regional electrophilicity

[*] Dr. Z. Wang,[+] Y. Wang,[+] Prof. K. Davey, Prof. Z. Guo
School of Chemical Engineering & Advanced Materials,
The University of Adelaide
Adelaide, SA 5005 (Australia)
E-mail: zaiping.guo@adelaide.edu.au

Dr. Z. Wang,[+] Prof. Z. Guo
Institute for Superconducting & Electronic Materials, Australian Institute for Innovative Materials, University of Wollongong
Wollongong, NSW 2522 (Australia)

Dr. J. Lu
Argonne National Laboratory
Lemont, IL 60439 (USA)
E-mail: junlu@anl.gov

Prof. B. Li
Shenzhen Key Laboratory on Power Battery Safety and Shenzhen Geim Graphene Center, Tsinghua Shenzhen International Graduate School, Tsinghua University
Shenzhen 518055 (China)
E-mail: libh@sz.tsinghua.edu.cn

Dr. J. C. Bouwer
Molecular Horizons and School of Chemistry and Molecular Bioscience, Illawarra Health and Medical Research Institute, University of Wollongong
Wollongong, NSW 2522 (Australia)

[+] These authours contributed equally to this work.

(Figure 1a). The polarization degree of solvent molecules can be reduced via introduction of anions into the solvation sheath (Figure 1a), leading to lower possibility of accepting electrons. It is reported for Li-ion batteries that constructing Li coordination structure with solvated anions is more important than forming a SEI to improve the stability of graphite anode.[18] With concentrated and high salt-to-solvent ratio electrolytes for LMBs, anions participate in Li^+ solvation.[7,19] The improved electrochemical performance of these electrolytes is usually associated with reduced free solvent molecules and the formation of anion-derived solid-electrolyte interphase (SEI), however, the contribution of anions in solvation sheath in improving the stability of electrolyte against Li metal has been overlooked. Given the intrinsic disadvantages of high-salt-containing electrolytes, it would be practically attractive if anions could be introduced into solvation sheath of Li^+ without the expense of increasing viscosity and reducing ionic conductivity. It appears that where the electrostatic attraction between anions and solvents molecules to Li^+ reaches a "delicate" balance, the existence of anion in solvation sheath can be practically realized.[17] Gutmann donor number (DN) is a widely accepted parameter to measure ability of compounds to act as electron donors.[20] It can be used as a scale to assess the attraction between Li^+ and other electrolyte components.[21] It is hypothesized that when anions and solvents with comparable DN are selected (Table S1 and Figure S1), anions can readily get into solvation sheaths which helps to improve reduction stability of the electrolyte.

Here, to test this hypothesis we selected nitrate anion (NO_3^-) with DN of 22.2 kcal mol^{-1} and trimethyl phosphate (TMP) (DN = 23.0 kcal mol^{-1}) as electrolyte components by adding $LiNO_3$/TMP solution into carbonate electrolyte. The existence of TMP weakens the electrostatic attraction between Li^+ and NO_3^-, but it is insufficient to "free" NO_3^-. Consequently, the interaction amongst TMP, NO_3^- and Li^+ reaches a balance and NO_3^- is introduced into the solvation structure. In this designed electrolyte, because of the involvement of NO_3^-, the electrophilicity of both coordinated carbonate and TMP molecules in the solvation structure is reduced, suppressing solvent decomposition on Li. Importantly, this electrolyte is non-flammable with a zero self-extinguishing time. It also exhibits low viscosity (4.04 mPa s^{-1}) and high ionic conductivity (5.42 mS cm^{-1}). The reversibility of the Li plating/stripping in Li-Cu cells is boosted to 99.49 %, one of the highest reported for non-

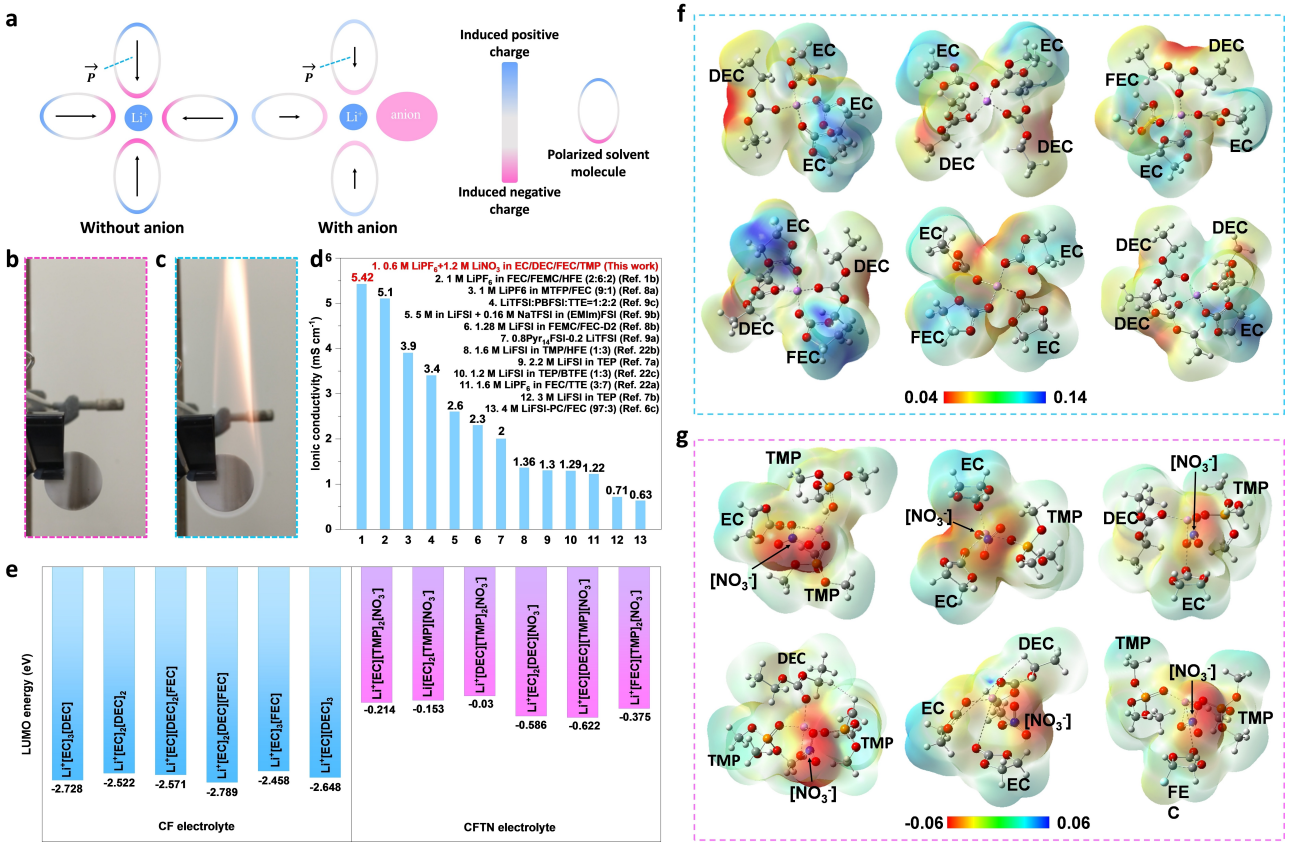

Figure 1. Physical and chemical properties of the electrolyte. a) Schematic for Li^+ solvation structure and polarity effects of solvent molecules. The deeper-color represents higher polarity degree. $\vec{P}$ is the internal induced electric field of solvent molecules. The presence of anions in the Li^+ solvation clusters reduces the polarity degree of solvent molecules. Flame test for CFTN electrolyte (b) and CF electrolyte (c); d) Ionic conductivity of CFTN and comparison with state-of-the-art non-flammable electrolytes for LMBs; e) LUMO energy values for representative Li^+ solvation clusters in CF and CFTN; Electrostatic potential (ESP) analysis for representative Li^+ solvation clusters in CF electrolyte (f) and CFTN electrolyte (g).

flammable electrolytes. The lifespan of LMBs with lean electrolyte is significantly extended despite harsh conditions with mass loadings of, respectively, 14.3 mg cm^{-2} and 16.7 mg cm^{-2} for lithium iron phosphate (LFP) and lithium nickel manganese cobalt oxide cathodes ($LiNi_{0.8}Co_{0.1}Mn_{0.1}O_2$, NCM811) and n/p ratio <5. Findings will be of immediate benefit for design for safe and high-performance LMBs.

Results and Discussion

The electrolyte is formulated by mixing 60 vol. % carbonate electrolyte, 1 M $LiPF_6$ in ethylene carbonate (EC)/ diethyl carbonate (DEC)/fluoroethylene carbonate (FEC) in a volume ratio of 4:4:2, with 40 vol. % 3 M $LiNO_3$/TMP. The concentration of $LiPF_6$ and $LiNO_3$ in the as-formulated electrolyte (denoted as CFTN) is 0.6 M and 1.2 M, respectively. The electrolyte without TMP and $LiNO_3$ (0.6 M $LiFP_6$ in EC/DEC/FEC = 4:4:2) (denoted as CF), and other electrolytes with varying concentration of TMP and $LiNO_3$ were used as references, as listed in Table S2.

The CFTN was clear and transparent without apparent sediment or impurity (Figure S2). Significantly the CFTN electrolyte could not be ignited by lighter because it exhibits a self-extinguishing time of 0 s g^{-1} (Figure 1b, Figure S3 and Video S1), which is attributed to the use of 40 % TMP in the solvent. In contrast, the CF and other reference carbonate electrolytes without TMP are highly flammable with a self-extinguishing time of >60 s g^{-1} as was confirmed via flame test (Figure 1c, Figure S3 and Videos S2–S5). The ionic conductivity of the CFTN electrolyte was determined to be 5.42 mS cm^{-1} (Figure 1d and Figure S4) which is a greater value than for many non-flammable electrolytes (Table S3).[6c,7,8,9,22] The viscosity of CFTN electrolyte is 4.04 mPa s^{-1}, a value significantly less than that for concentrated, high salt-to-solvent, and ionic liquid non-flammable electrolytes (Figure S5).[6c,7,9] The advantage of ionic conductivity and viscosity of CFTN are attributed directly to the relatively low salt concentration, together with the size of NO_3^- anion as it is significantly smaller than that of widely used bis(fluorosulfonyl)imide anion (FSI^-) and bis-(trifluoromethanesulfonyl)imide anion ($TFSI^-$). In addition, the high ionic conductivity of $LiPF_6$ salt, the low viscosity of both DEC and TMP, and the appropriate size of NO_3^- guarantee the superior physical properties of the designed electrolyte.

To study the thermodynamic stability of the electrolyte against Li, the structures of both CF and CFTN electrolytes were simulated by ab initio molecular dynamics (MD) (Figure S6). In the CF electrolyte, four (4) carbonate molecules coordinate with one (1) Li^+, and the computed LUMO energy values for representative solvated Li^+ clusters ranged from -2.789 to -2.088 eV (Figure 1e and Figure S7). These values are significantly less than those for free molecules, which confirms that with the solvation the reduction stability of solvated solvents was reduced, facilitating decomposition of electrolyte.[16] The situation is different with CFTN as it results from a competition between solvent molecules and anions in contesting for Li^+, both solvent (TMP and carbonate) molecules and NO_3^- coordinate with Li^+ in solvation. Because the DN of TMP and NO_3^- are similar, both fail to take possession of Li^+ completely and coexist. Additionally, TMP accounts for 56.5 % of the solvent molecules in the solvation sheaths, greater than that for carbonates of 43.5 %, despite the molar ratio of TMP in electrolyte solvent being 32.19 % (Table S4). This is because TMP has a greater DN of 22.2 kcal mol^{-1} compared with EC (16.4 kcal mol^{-1}), DEC (16.2 kcal mol^{-1}) and FEC (9.1 kcal mol^{-1}) (Table S1 and Figure S1). Therefore, it preferentially coordinates with Li^+. The LUMO energy values for representative Li^+ solvation clusters range from -0.622 to -0.03 eV, values that are greater than that for CF (Figure 1f and Figure S8). The increased LUMO energy values are attributed to the presence of salt anions in the Li^+ solvation clusters.

The electrostatic nature of Li^+ solvation clusters can be readily visualized through electrostatic potential (ESP) mapping that represents the electrophilicity on the surface of solvent molecules. For the six (6) representative Li^+ solvation clusters in CF (Figure 1g and Figure S9), the EC molecules exhibit a more positive ESP value and are colored as deeper-blue. This finding reflects that more positive charges are distributed on the outer end of the EC molecule (away from Li^+). Because of its large molecular polarizability EC works as a good solvent to separate the cations and anions of Li salt. However, its polarity induced by Li^+ in turn, puts it in a position of accepting electrons and therefore decomposition, something experimentally demonstrated.[23] In contrast, with the presence of NO_3^- anions the Li^+ solvation clusters in CFTN exhibit universally lower ESP values (Figure 1f and Figure S10), especially for EC and DEC molecules. This finding confirms that the solvent molecules in the presence of NO_3^- have less induced positive charges and lower degree of polarity. TMP, widely regarded as an unstable component against Li metal, was computed to have a lower ESP value than carbonate molecules, which means that its decomposition priority is inferior to carbonates. Both the improved LUMO energies and decreased ESP values confirm that the overall stability of Li^+ solvation clusters in the electrolyte have been significantly boosted, which contributes to the electrochemical performance of LMBs.

Theoretically, the stability between electrolyte and Li metal is reflected in the reversibility of Li metal anode during electrochemical cycling and is assessed quantitatively via Coulombic efficiency (CE) in Li-Cu cells.[24] As is shown in Figure 2a, the Li-Cu cell using CFTN electrolyte exhibits a high average CE of 99.49 % at 0.25 mA cm^{-2}, a value that is amongst the greatest in reported findings in non-flammable electrolytes. In comparison, the CE values for Li-Cu cells using CF electrolyte and other typical carbonate-based electrolytes are less (Figure 2a, Figures S11 and S12). Even at a high current density of 3 mA cm^{-2} and a high capacity of 3 mAh cm^{-2}, the Li-Cu cell using CFTN electrolyte delivers a CE of $\approx$98 % (Figure S13), comparable to that achieved in an outstanding liquid–gas electrolyte.[25] In the non-flammable electrolyte without $LiNO_3$ (0.6 M $LiPF_6$

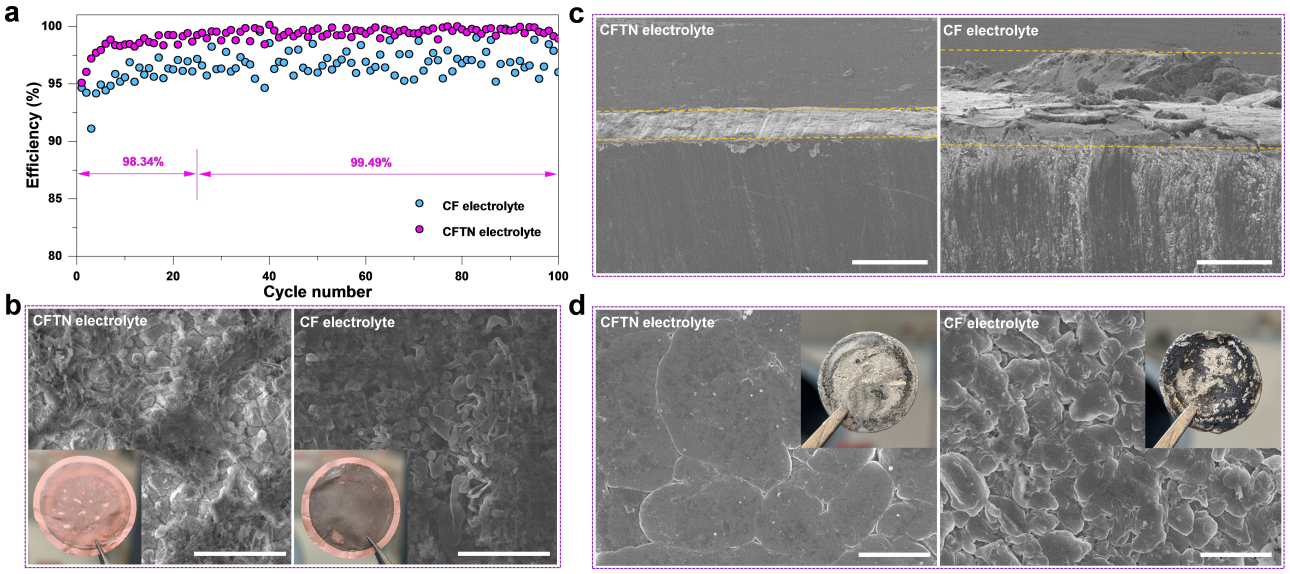

Figure 2. Improving Li plating/stripping reversibility. a) Coulombic efficiency (CE) for Li-Cu cells using CFTN and CF electrolytes with fixed capacity of 1 mAh cm^{-2} under current density 0.25 mA cm^{-2}; b) SEM images and optical images (insets) of Cu-foil after the 5th Li stripping; c) Cross-sectional SEM images of Li electrodes cycled in CFTN and CF; d) Top-view (plan) SEM images of Li electrodes cycled in CFTN and CF. The Li electrodes were cycled for 50 cycles with a capacity of 1 mAh cm^{-2}. Scale bars: 10 μm (b); 200 μm (c) and 5 μm (d).

in EC/DEC/FEC/TMP), the CE falls rapidly during cycling (Figures S11 and S12). These results underscore that the $LiNO_3$ in CFTN restrains the side reaction between TMP and Li metal, and boosts stability of the basic carbonate electrolyte. Given the total concentration of Li^+ in CFTN is 1.8 M, the $LiPF_6$ concentration in carbonate and carbonate-phosphate electrolytes is increased to 1.8 M to exclude the concentration effect. The CE of Li-Cu cell in carbonate and carbonate-phosphate electrolytes with 1.8 M $LiPF_6$ does not show any apparent improvement (Figures S14 and S15), confirming that positive effect of NO_3^-. Additionally, when decreasing the concentration of $LiNO_3$ in the electrolyte, the CE for Li-Cu cells declines (Figure S16), highlighting that the more $LiNO_3$ added, the greater the stability of electrolyte that can be achieved. Based on these findings, the excellent CE for CFTN is ascribed to the positive role of NO_3^- in the solvation structure that reduces the ESP values for TMP and EC and reduces reaction with metallic Li. Introducing anion into Li^+ solvation sheaths via selecting solvent with similar DN to that of NO_3^- results in beneficial effects. This proof-of-concept is also confirmed in the pair of $CF_3SO_3^-$ (OTF^-) and EC, with similar DN values of 16.9 and 16.4 kcal mol^{-1}, respectively. It is widely acknowledged that ethers including, dimethoxymethane (DME) and tetrahydrofuran (THF), exhibit significantly better stability against Li metal than EC (a typical carbonate). However, EC has unique advantages when paired with LiOTF. As is shown in Figure S17, when using DME or THF as single solvent, the CE of relevant Li-Cu cells is far from satisfactory. However, the Li-Cu cells in electrolyte with EC exhibit significantly more stable CE with cycling, and the average CE increases at greater EC ratio. Because of the different DN value (20 kcal mol^{-1}) of solvent compared with that for OTF^- (16.9 kcal mol^{-1}), OTF^- anions are not significantly involved in the solvation sheath of Li^+ in DME or THF electrolyte and exist as "free" anions. By adding a co-solvent, i.e., EC with similar DN value (16.4 kcal mol^{-1}) to that for OTF^-, OTF^- gets into solvation sheaths. This reduces the activity of solvent molecules in the solvation sheath, and thereby suppresses solvent decomposition. It is concluded the electrolyte with EC as co-solvent therefore delivers significantly boosted electrochemical performance.

To confirm visually the high reversibility of Li metal anode in CFTN, the Cu foils following Li stripping were investigated with a scanning electron microscopy (SEM). As is shown in Figure 2b, Figures S19 and S20, only a few thin-film-like residuals are exhibited on Cu-foil following Li stripping in CFTN that are the unavoidable formation of SEI. In contrast, the Cu-foil after Li stripping in CF electrolyte has significantly denser irreversible residual coating with tubular Li left (Figure 2b, Figures S19 and S20). The optical images of Cu foils following Li plating/stripping cycles confirmed that less "dead" and electrochemically inactive Li is formed in the CFTN electrolyte (insets for Figure 2b). The morphology of cycled Li metal electrodes in Li-Cu cells for 50 cycles was investigated where the Li cycled in CFTN was denoted Li-CFTN and that in CF electrolyte Li-CF. As is shown in the cross-sectional SEM images of Figure 2c and Figure S21, a dense layer of "activated" Li is observed on Li-CFTN, whilst there is a thick-spongy layer of dead Li with apparent cracks on Li-CF. The top-view (plan) SEM images (Figure 2d and Figure S22) show a denser and flatter surface for the Li-CFTN compared with that for Li-CF. The Li-CFTN retains relatively shiny metallic lustre, whereas most of the surface of Li-CF is covered with black-color Li deposits (inset Figure 2d) due to the presence of dead Li.

To confirm the effect of CFTN on stabilizing Li metal anode, Li||Li symmetric cells with thin Li foil (50 μm) were tested at a high current density 4 mA cm^{-2} and high area capacity 4 mAh cm^{-2}. As is seen in Figure S23, the Li||Li cell with CF exhibits a "sharp" increase in voltage polarization with cycling, and short-circuits after 62 h because of Li dendrite growth and depletion of electrochemically active Li. In contrast, the Li||Li cell with CFTN remains stable for >160 h, confirming a higher Li anode reversibility and more stable electrolyte-electrode interface.

Because the decomposition of electrolyte on Li can be investigated via analysis of surface chemistry of Li metal electrodes, X-ray photoelectron spectroscopy (XPS) depth-profiling was applied to determine the components and distributions along the thickness-direction for Li-CFTN and Li-CF. As is shown in the Li 1s spectra for Li-CFTN, an apparent peak for metallic Li (Li^0) appears following sputtering for 100 s with intensity becoming stronger in the following sputtering (Figure 3a). In a sharp contrast, the Li^0 peak for Li-CF remains weak despite after sputtering for 300 s. This finding confirms that the SEI formed on Li-CFTN during Li plating/stripping cycles is significantly much less (thinner) than that for Li-CF. For Li-CFTN, the organic ROCOOLi (where R is a low-molecular-weight alkyl group[26]) distributes on its surface, and its content decreases during sputtering. Importantly, it was also observed that inorganic components, including Li_3N, LiF and Li_2O, became dominant in the inner side of the SEI. The FEC in CFTN electrolyte contributes fluorinated SEI layer, which is beneficial to passivate Li metal surface. The addition of

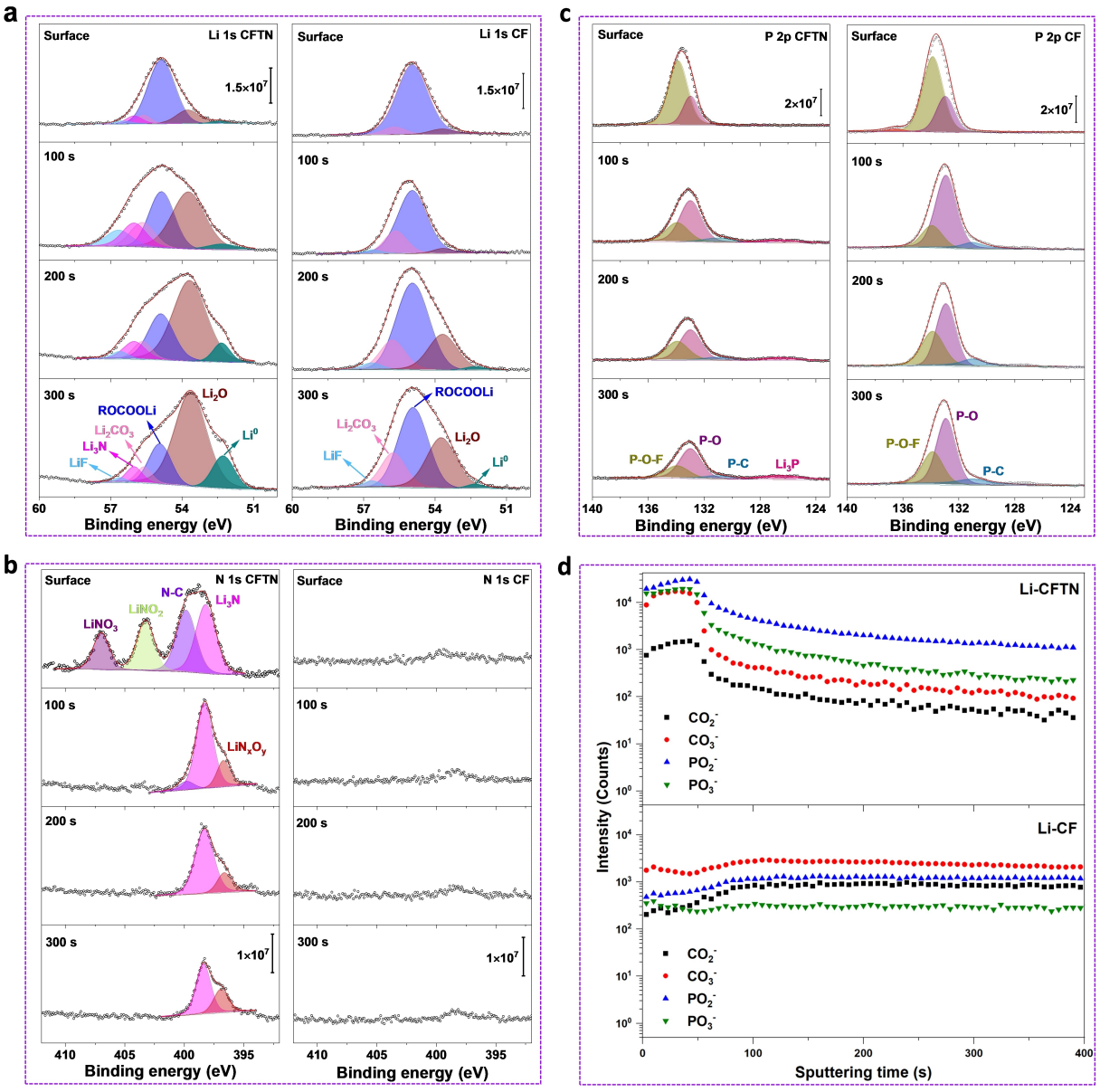

Figure 3. Alleviating reductive decomposition of electrolyte on Li. a)–c) X-ray photoelectron spectroscopy (XPS) depth-profile spectra for Li 1s (a), N 1s (b), and P 2p (c) for the Li cycled in CFTN and CF electrolyte; (d) Time of flight, secondary ion mass spectroscopy (TOF-SIMS) depth profiles for CO_3^- and CO_2^-, and PO_2^- and PO_3^- in Li cycled in CFTN and CF.

$LiNO_3$ into the electrolyte brings high-quality species into the Li-electrolyte interface in the form of Li_3N and LiN_xO_y (Figure 3b). These are reported to be excellent ionic conductors that lead to optimized Li deposition morphology. For Li-CF however, the major component in its SEI during the 300 s sputtering is ROCOOLi (Figure 3a). The Li_2CO_3 content increases along the depth-direction and its peak intensity is greater than that in Li-CFTN. The C 1s spectra (Figure S24) confirm that appreciably more ROCOOLi and Li_2CO_3 are formed on Li-CF. This finding is in very good agreement with that obtained on time-of-flight secondary ion mass spectrometry (TOF-SIMS). As is shown in the TOF-SIMS depth profile of Figure 3d, the counts for CO_3^- and CO_2^- secondary ions that represent ROCOOLi or Li_2CO_3, significantly decline following sputtering for 60 s in Li-CFTN, whilst in Li-CF the counts for CO_3^- and CO_2^- secondary ions show no apparent change despite following a 400 s sputtering. Both the formation of ROCOOLi and Li_2CO_3 are attributed to the decomposition of carbonates.[26,27] The unstable ROCOOLi would further decomposes to Li_2CO_3.[28] Although Li_2CO_3 is common and difficult to eliminate, it is unwanted in the SEI layer because of its poor Li^+ ion conductivity, ability in cutting-off electron tunnelling, and possibility of gas generation.[29] Taking this into consideration, alleviating the decomposition of carbonates as far as possible is of significant meaning.

In the P 2p XPS depth profile (Figure 3c), the amount of P-containing components for Li-CFTN is significantly less than that for Li-CF. In addition, the peak intensity of the P 2p XPS spectra for Li-CFTN reduces significantly with sputtering, however for Li-CF the peak intensity remains as strong as its initial value following 300 s sputtering. This evidences that less P-containing species are formed in Li-CFTN. A similar trend was found in the TOF-SIMS depth profile in Figure 3d. The count for PO_2^- and PO_3^- secondary ions (representing the decomposition products of P-containing components in the electrolyte) for Li-CFTN declines apparently after sputtering for $\approx$60 s, but that for Li-CF has no apparent change despite sputtering for 400 s. Importantly, considering that the same amount of $LiPF_6$ was used in both electrolytes but an additional 40 % TMP was used as the solvent for CFTN electrolyte, we conclude therefore that the side reactions between TMP and Li metal have been suppressed. It is reported that as little as 5 % of TMP addition results in performance decline,[13,14] however in CFTN electrolyte the CE for Li-Cu cell is boosted significantly, even if the TMP in solvent is as high as 40 %, confirming the effects of solvated NO_3^- on suppressing the decomposition of electrolyte (including TMP). It is seen that the P–O–F peaks for Li-CFTN are smaller than those in Li-CF (Figure 3c), and the peak for $LiP_xO_yF_z$, which is observed in Li-CF, is not found in the F 1s spectra for Li-CFTN (Figure S25), evidencing the decomposition of $LiPF_6$ was also alleviated.

During Li deposition, grain-growth behaviour significantly relies on the mass diffusion mechanism through the Li-electrolyte interface. The components and structure of SEI result from the reaction of electrolyte and Li and directly impact the morphology of Li, which impact the reversibility of Li metal anode. The SEM images of Figures 4a,b (and Figure S26) exhibit the significant differences in deposited Li in CFTN and CF electrolyte. In the initial nucleation stage, Li^+ deposits into spherical particles in CFTN electrolyte, but in finely fibrous shape in CF electrolyte. In later grain-growth (Figure S27) the Li particles in CFTN exhibit uniform growth, and finally grow into larger "chunky" grains. In contrast however, the Li growth in CF exhibits selective direction, namely, it grows faster along its length and slower in diameter direction.

To determine the mass diffusion mechanism, cryogenic transmission electron microscopy (cryo-TEM) was used to analyse the SEI layer formed on the initially deposited Li.[30] Low magnification cryo-TEM images of Li particles obtained from CFTN and CF electrolyte were consistent with corresponding SEM images (Figures 4c,d). The chunky Li grown in CFTN electrolyte has a wave-like SEI without a clear boundary between Li and SEI, as is seen in Figure S28. There is instead a gradual transition from SEI layer to Li metal, Figure 4e. A similar phenomenon was found for other $LiNO_3$-containing electrolytes.[31] The high magnification images are presented in Figures 4e,f. By indexing the lattice fringes and fast Fourier transform (FFT) patterns in enlarged images (Figure 4e and Figure S29) the crystalline phases in the representative area were confirmed as Li_3N, LiN_xO_y and residual $LiNO_3$. Both the Li_3N and LiN_xO_y have high ionic conductivity and provide rapid Li^+ diffusion channels through the SEI layer[19a,32] so that Li^+ is transported readily and the grain-growth is isotropic (Figure 4g). Interestingly, no crystalline Li_2O and/or LiF phases are apparent in the representative area, despite being detected on the surface of the cycled Li. This finding is likely because the Li_2O and LiF formed in CFTN electrolyte is non-crystalline and mixed with the amorphous matrix of the SEI. In an enlarged cryo-TEM image of Li deposited in CF electrolyte, a SEI layer with thickness of $\approx$14 nm can be seen (Figure S28). The top layer of SEI (close to vacuum) is crystalline Li_2CO_3, whilst the inner layer is amorphous matrix mixed with crystalline Li_2CO_3 phase (Figures 4f and S30). Importantly, beneath the SEI layer, some crystalline "islands" with an average size of a few nanometers distributed inside Li, that can be readily identified as Li_2CO_3 and Li_2O. Both Li_2CO_3 and Li_2O have poor ionic conductivity, therefore Li^+ diffusion through the interface is sluggish, it leads to uneven Li^+ flux and one-dimensional dendritic growth of deposited Li (Figure 4h). These cryo-TEM findings confirm that the decomposition of carbonates is suppressed, and the SEI layer containing both nitrided and fluorinated species is more effective in regulating Li morphology than the SEI layer with fluorinated species only.

The improved kinetics during Li deposition were confirmed via electrochemical testing. As is seen in Figure S31, the exchange current density (i_0) calculated from the Tafel plots in CFTN is 0.719 mA cm^{-2}, which is > more than four (4) x times greater than that in CF of 0.155 mA cm^{-2}. Additionally, the electrochemical impedance of Li||Li cells cycled in CFTN is significantly less than that cycled in CF (Figure S32).

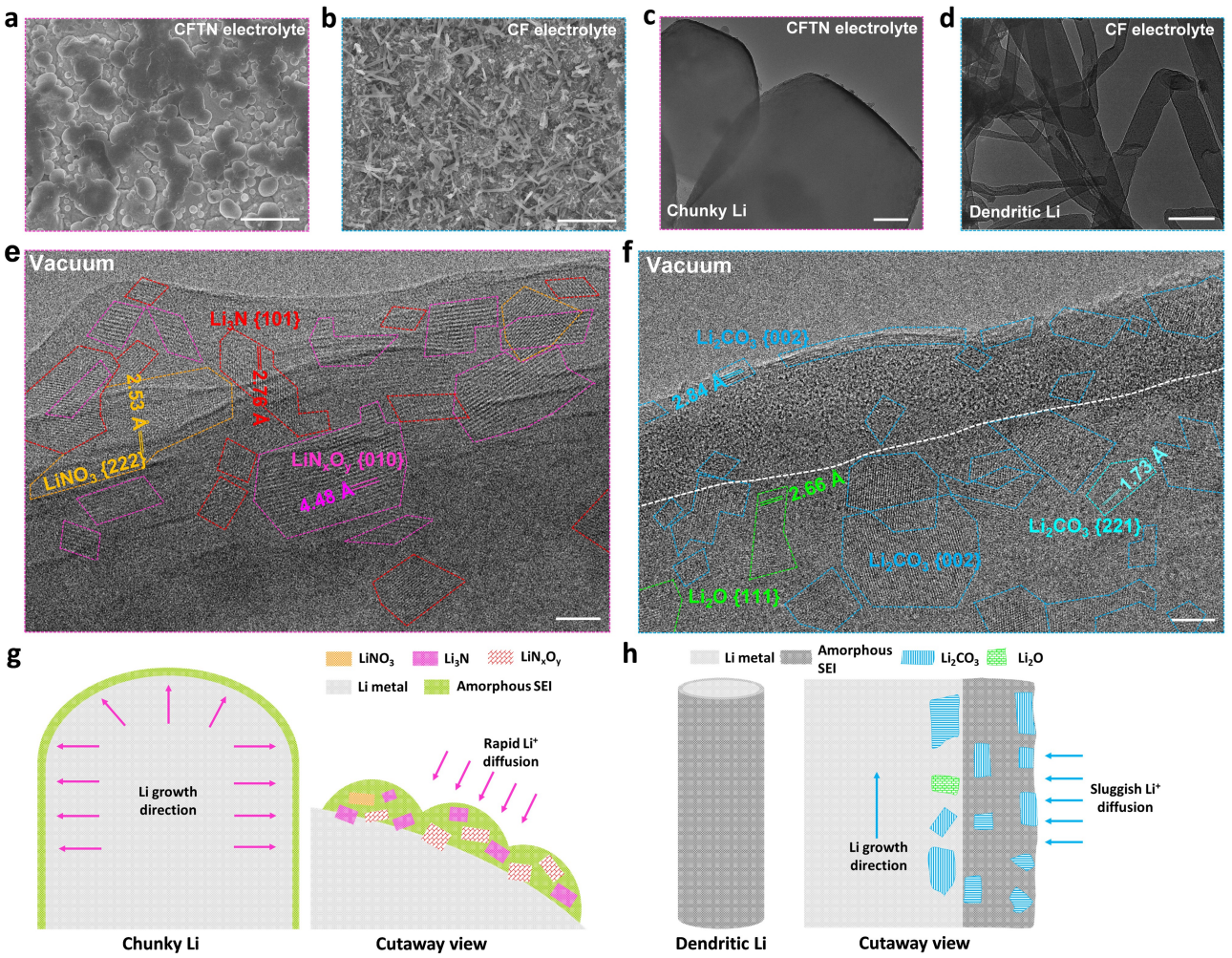

Figure 4. Regulating Li morphology. SEM images of Li deposited in CFTN (a) and CF (b); Low-magnification cryo-TEM images of Li deposited in CFTN (c) and CF (d); High-magnification cryo-TEM image of Li deposited in (e) CF and (f) enlarged cryo-TEM image of SEI. Boundary between SEI and Li is shown as a white-colour dashed line in (f). Scale bar is 5 nm. Schematic for Li growth and impact of ionic conductivity in (g) CFTN and (h) CF.

Compared with dendritic Li formed in CF, the chunky Li formed in CFTN electrolyte has increased particle size, and minimal, microstructural tortuosity that aids suppression of dendrite growth and reduces the formation of dead Li.[31b,33] Additionally, the enlarged-size decreases the specific surface of deposited Li and thereby reduces side reactions of electrolyte on the Li surface. Therefore, the reversibility of Li metal anode during plating/stripping cycles is boosted.

Li metal full cells with LFP or NCM811 as cathodes were tested to assess performance of CFTN electrolyte. Cycling performance of the LFP||Li-foil and NCM811||Li-foil cells with flooded electrolyte (60 μL) and high cathode mass loading were evaluated. As is shown in Figure S33, the LFP||Li-foil cell using CFTN electrolyte retains a capacity of 80 % despite 800 cycles, whilst that using CF electrolyte exhibits significant capacity decay after 500 cycles. Similarly, the lifespan for NCM811||Li-foil cells with CFTN electrolyte (>300 cycles) is greater than that with CF electrolyte (≈200 cycles) (Figure S34). To achieve high energy density, practical LMBs must operate with lean electrolyte, high cathode capacity together with a low n/p ratio (capacity ratio of the negative electrode to positive electrode). Therefore, high mass-loading LFP (≈14.3 mg cm^{-2}) (2.43 mAh cm^{-2}) and NCM (≈16.7 mg cm^{-2}) (4.75 mAh cm^{-2}) electrodes and a limited capacity of Li were used in the Li metal full cells, and the electrolyte was fixed at ≈10 μL mAh^{-1}. As is shown in Figure 5a (and Figure S35) when n/p ratio is controlled at 5, the LFP||Li battery using CFTN electrolyte exhibited a high initial CE (ICE) of 98.9 % at 0.2 C (≈0.48 mA cm^{-2}), greater than that for LFP||Li battery using CF electrolyte (97.8 %). Both the CE and discharge capacity for LFP||Li battery using CF electrolyte highly significantly decreased following 60 cycles. Importantly however, those for LFP||Li battery using CFTN electrolyte remained stable. Despite 150 cycles the LFP||Li battery using CFTN exhibited a high discharge capacity of 121.3 mAh g^{-1} with capacity retention of 81.6 %. When the n/p ratio was reduced to 2, as is shown in Figure 5b and Figure S36, the ICE for LFP||Li battery using CFTN (99.03 %) was greater than that using CF (96.69 %). The CE and capacity of the LFP||Li battery

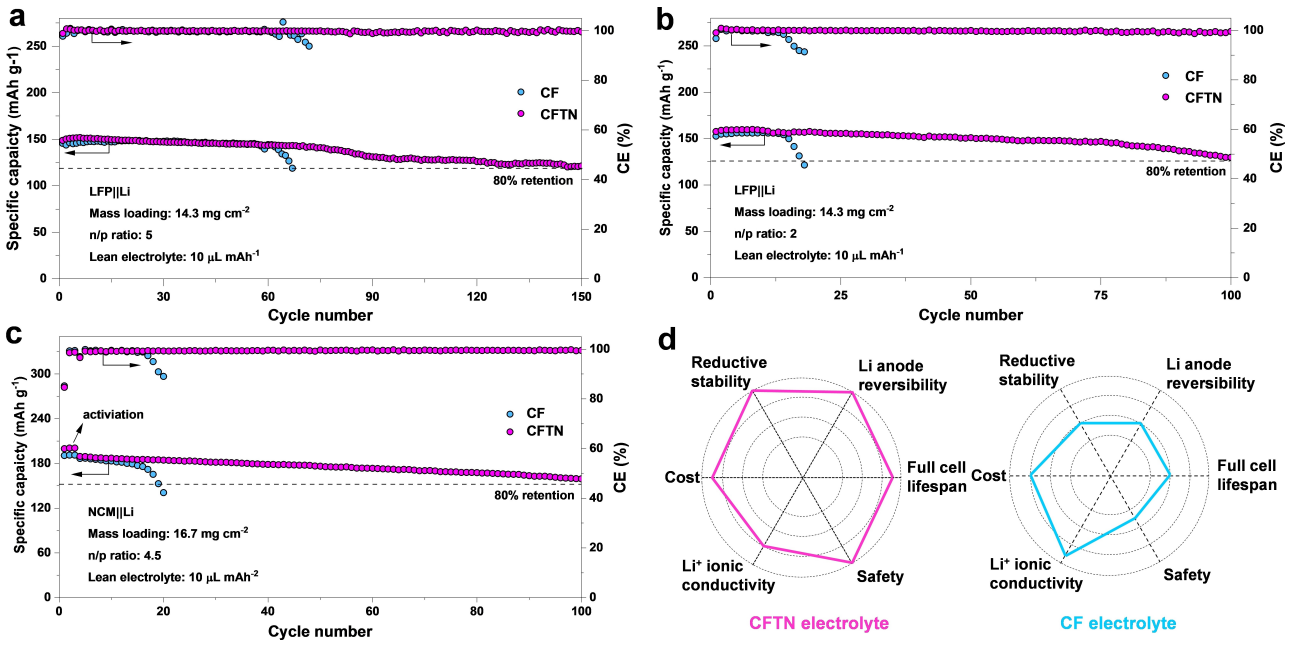

Figure 5. Practical application of the electrolyte. LFP||Li full cell tests under high cathode loading and lean electrolyte with n/p ratio of 5 (a) and 2 (b) at 0.2 C (≈0.48 mA cm^{-2}). c) NCM||Li cell test under high cathode loading and lean electrolyte with n/p ratio of 4.5 in which the batteries were activated at 0.05 C and cycled at 0.1 C (≈0.47 mA cm^{-2}); d) Comparison of properties and performance of CFTN and CF. Axes in the hexagons represent relative comparisons of properties and performance, with those superior plotted outermost.

using CF electrolyte reduced rapidly within 20 cycles. Significantly however the LFP||Li battery using CFTN continued for >100 cycles with high capacity retention of 82.3 % at 0.2 C (≈0.45 mA cm^{-2}). When the CFTN electrolyte was applied in an NCM811||Li battery with an n/p ratio of 4.5 the battery retained more than 80 % of its capacity after 100 cycles at 0.1 C (≈0.47 mA cm^{-2}), whilst the capacity of the NCM811||Li battery with CF rapidly decayed to <80 % within 20 cycles (Figure 5c and Figure S37).

In harsh conditions the capacity decay of the full cell can be mainly explained as follows, there is: 1) insufficient Li^+ transport ability of the electrolyte to transfer all the necessary Li^+ into and out from the relatively thick LFP/NCM electrodes, and 2) depletion of electrolyte, or active Li, because of side reactions. CFTN electrolyte has a low viscosity and high ionic conductivity and therefore the capacity for high mass loading cathode to be delivered. Its boosted compatibility with Li ensures that the consumption of both active Li and electrolyte is minimized. We conclude therefore the lifespan of full cells using CFTN electrolyte will be extended.

In addition to boosted stability against Li metal, it was found that CFTN suppresses structure degradation of NCM811 cathode during battery cycling. As is shown in the scanning transmission electron microscopy (STEM) images of Figure S38, for the NCM811 cycled in CFTN, the accumulated disordered rock salt phase (cation mixing layer) resulting from the electrolyte-electrode interaction[34] is 3–4 nm, whilst that for NCM811 cycled in CF is significantly greater at 7–9 nm. This improved surface property also help to extend the lifespan of the NCM811||Li cell.

The energy density for LFP||Li and MCM811||Li cell on electrode-level (based on total mass of cathode and anode) was calculated to be 445 and 629 Wh kg^{-1}, respectively. Given the relative harsh testing conditions especially high cathode loading and lean electrolyte, it is concluded that the energy density and lifespan of full cells with CFTN electrolyte are comparable with, or superior, to reported non-flammable electrolytes (Table S5).

The estimated cost of the CFTN electrolyte is significantly less than that for those of reported high-performance electrolytes, including concentrated, high salt-to-solvent ratio and all-fluorinated non-flammable electrolytes (Figure S39 and Tables S6 and S7). The boosted reduction stability, Li anode reversibility, full cell lifespan, and safety, together with its appropriate physical properties and low cost (Figure 5d), underscores that CFTN electrolyte is comprehensive and has practical potential for commercialization.

Conclusion

The thermodynamic stability of electrolyte is significantly increased by introducing anions into solvation sheaths via selecting anions and solvents with comparable DN values. Using NO_3^- and TMP as an example, we have demonstrated a high-performance non-flammable electrolyte. The solvated NO_3^- reduces the polarization degree of solvent molecules, as theoretically evidenced by the more positive ESP values, and promoted LUMO energies for the Li^+ solvation structure. XPS, TOF-SIMS and cryo-TEM findings experimentally confirm that the side reaction between the electro-

lyte (especially carbonate and TMP solvents) and Li are supressed. A major benefit is that depletion of both electrolyte and Li metal anode is minimized to boost the performance of LMBs at lean electrolyte and low n/p ratio. The rational design of electrolyte appears generalizable and therefore could be practically extended to other alkali-metal batteries. Findings will be of immediate benefit to researchers and manufacturers in design of electrolytes for practically safe, high-performance alkali metalbatteries.

Acknowledgements

Financial support provided by the Australian Research Council (ARC) (LP160101629, DP210101486, DP200101862, 180100141, and FL210100050) is gratefully acknowledged. Z.W. and Y.W. acknowledge the Chinese Scholarship Council for scholarship support (No. 201706340049 and No. 201808440447). The work at Argonne was supported by the U.S. Department of Energy (DOE), Office of Energy Efficiency and Renewable Energy, Vehicle Technologies Office. Argonne National Laboratory is operated for the U.S. DOE, Office of Science, by UChicago Argonne, LLC, under Contract No. DE-AC02-06CH11357. The authors thank Drs. Chao Wu, Wilford Lie, and Tania Silver at UOW for helpful discussions. The authors thank Dr. Songyan Yin, Surface Analysis Laboratory, UNSW for assistance with TOF-SIMS testing. The authors gratefully acknowledge the use of the University of Wollongong Cryogenic Electron Microscopy Facility at Molecular Horizons. Open Access publishing facilitated by The University of Adelaide, as part of the Wiley - The University of Adelaide agreement via the Council of Australian University Librarians.

Conflict of Interest

The authors declare no conflict of interest.

Data Availability Statement

The data that support the findings of this study are available from the corresponding author upon reasonable request.

Keywords: High Coulombic Efficiency · High Stability · Li Metal Battery · Non-Flammable Electrolyte

[1] a) D. Lin, Y. Liu, Y. Cui, *Nat. Nanotechnol.* **2017**, *12*, 194; b) X. Fan, L. Chen, O. Borodin, X. Ji, J. Chen, S. Hou, T. Deng, J. Zheng, C. Y. Yang, S. C. Liou, K. Amine, K. Xu, C. S. Wang, *Nat. Nanotechnol.* **2018**, *13*, 715; c) L. Suo, W. Xue, M. Gobet, S. G. Greenbaum, C. Wang, Y. Chen, W. Yang, Y. Li, J. Li, *Proc. Natl. Acad. Sci. USA* **2018**, *115*, 1156; d) Y. Wang, Z. Wang, L. Zhao, Q. Fan, X. Zeng, S. Liu, W. K. Pang, Y.-B. He, Z. Guo, *Adv. Mater.* **2021**, *33*, 2008133; e) Z. Wang, Y. Wang, Z. Zhang, X. Chen, W. Lie, Y.-B. He, Z. Zhou, G. Xia, Z. Guo, *Adv. Funct. Mater.* **2020**, *30*, 2002414; f) Q. Ma, J. Yue, M. Fan, S.-J. Tan, J. Zhang, W.-P. Wang, Y. Liu, Y.-F. Tian, Q. Xu, Y.-X. Yin, Y. You, A. Luo, S. Xin, X.-W. Wu, Y.-G. Guo, *Angew. Chem. Int. Ed.* **2021**, *60*, 16554; *Angew. Chem.* **2021**, *133*, 16690.

[2] a) D. Lisbona, T. Snee, *Process Saf. Environ. Prot.* **2011**, *89*, 434; b) J. Liu, Z. Bao, Y. Cui, E. J. Dufek, J. B. Goodenough, P. Khalifah, Q. Li, B. Y. Liaw, P. Liu, A. Manthiram, Y. S. Meng, V. R. Subramanian, M. F. Toney, V. V. Viswanathan, M. S. Whittingham, J. Xiao, W. Xu, J. Yang, X.-Q. Yang, J.-G. Zhang, *Nat. Energy* **2019**, *4*, 180; c) K. Brandt, *Solid State Ionics* **1994**, *69*, 173; d) M. Winter, B. Barnett, K. Xu, *Chem. Rev.* **2018**, *118*, 11433.

[3] a) S. Xia, X. Wu, Z. Zhang, Y. Cui, W. Liu, *Chem* **2019**, *5*, 753; b) O. Sheng, C. Jin, X. Ding, T. Liu, Y. Wan, Y. Liu, J. Nai, Y. Wang, C. Liu, X. Tao, *Adv. Funct. Mater.* **2021**, *31*, 2100891.

[4] a) Y. Jie, X. Ren, R. Cao, W. Cai, S. Jiao, *Adv. Funct. Mater.* **2020**, *30*, 1910777; b) S.-J. Tan, W.-P. Wang, Y.-F. Tian, S. Xin, Y.-G. Guo, *Adv. Funct. Mater.* **2021**, *31*, 2105253.

[5] Q.-K. Zhang, X.-Q. Zhang, H. Yuan, J.-Q. Huang, *Small Sci.* **2021**, *1*, 2100058.

[6] a) P. Shi, H. Zheng, X. Liang, Y. Sun, S. Cheng, C. Chen, H. Xiang, *Chem. Commun.* **2018**, *54*, 4453; b) Y. Yamada, J. Wang, S. Ko, E. Watanabe, A. Yamada, *Nat. Energy* **2019**, *4*, 269; c) S.-J. Cho, D.-E. Yu, T. P. Pollard, H. Moon, M. Jang, O. Borodin, S.-Y. Lee, *iScience* **2020**, *23*, 100844.

[7] a) Z. Zeng, V. Murugesan, K. S. Han, X. Jiang, Y. Cao, L. Xiao, X. Ai, H. Yang, J.-G. Zhang, M. L. Sushko, J. Liu, *Nat. Energy* **2018**, *3*, 674; b) L. Xiao, Z. Zeng, X. Liu, Y. Fang, X. Jiang, Y. Shao, L. Zhuang, X. Ai, H. Yang, Y. Cao, J. Liu, *ACS Energy Lett.* **2019**, *4*, 483.

[8] a) J. Holoubek, M. Yu, S. Yu, M. Li, Z. Wu, D. Xia, P. Bhaladhare, M. S. Gonzalez, T. A. Pascal, P. Liu, Z. Chen, *ACS Energy Lett.* **2020**, *5*, 1438; b) X. Fan, X. Ji, L. Chen, J. Chen, T. Deng, F. Han, J. Yue, N. Piao, R. Wang, X. Zhou, X. Xiao, L. Chen, C. Wang, *Nat. Energy* **2019**, *4*, 882; c) Z. Yu, H. Wang, X. Kong, W. Huang, Y. Tsao, D. G. Mackanic, K. Wang, X. Wang, W. Huang, S. Choudhury, Y. Zheng, C. V. Amanchukwu, S. T. Hung, Y. Ma, E. G. Lomeli, J. Qin, Y. Cui, Z. Bao, *Nat. Energy* **2020**, *5*, 526; d) X. Fan, L. Chen, X. Ji, T. Deng, S. Hou, J. Chen, J. Zheng, F. Wang, J. Jiang, K. Xu, C. Wang, *Chem* **2018**, *4*, 174.

[9] a) F. Wu, S. Fang, M. Kuenzel, A. Mullaliu, J.-K. Kim, X. Gao, T. Diemant, G.-T. Kim, S. Passerini, *Joule* **2021**, *5*, 2177; b) H. Sun, G. Zhu, Y. Zhu, M.-C. Lin, H. Chen, Y.-Y. Li, W. H. Hung, B. Zhou, X. Wang, Y. Bai, M. Gu, C.-L. Huang, H.-C. Tai, X. Xu, M. Angell, J.-J. Shyue, H. Dai, *Adv. Mater.* **2020**, *32*, 2001741; c) S. Lee, K. Park, B. Koo, C. Park, M. Jang, H. Lee, H. Lee, *Adv. Funct. Mater.* **2020**, *30*, 2003132.

[10] a) L. Suo, O. Borodin, T. Gao, M. Olguin, J. Ho, X. Fan, C. Luo, C. Wang, K. Xu, *Science* **2015**, *350*, 938–943; b) L. Suo, F. Han, X. Fan, H. Liu, K. Xu, C. Wang, *J. Mater. Chem. A* **2016**, *4*, 6639–6644.

[11] a) J. Xie, Z. Liang, Y. C. Lu, *Nat. Mater.* **2020**, *19*, 1006–1011; b) D. Dong, J. Xie, Z. Liang, Y. C. Lu, *ACS Energy Lett.* **2022**, *7*, 123–130.

[12] a) J. Wang, Y. Yamada, K. Sodeyama, E. Watanabe, K. Takada, Y. Tateyama, A. Yamada, *Nat. Energy* **2018**, *3*, 22; b) Q. Zheng, Y. Yamada, R. Shang, S. Ko, Y.-Y. Lee, K. Kim, E. Nakamura, A. Yamada, *Nat. Energy* **2020**, *5*, 291; c) J. Chen, A. Naveed, Y. Nuli, J. Yang, J. Wang, *Energy Storage Mater.* **2020**, *31*, 382.

[13] a) J. Yu, Y.-Q. Lyu, J. Liu, M. B. Effat, S. C. T. Kwok, J. Wu, F. Ciucci, *J. Mater. Chem. A* **2019**, *7*, 17995; b) X. Wang, E. Yasukawa, S. Kasuya, *J. Electrochem. Soc.* **2001**, *148*, A1058.

[14] a) K. Xu, M. S. Ding, S. Zhang, J. L. Allen, T. R. Jow, *J. Electrochem. Soc.* **2003**, *150*, A161; b) M. Morita, Y. Niida, N. Yoshimoto, K. Adachi, *J. Power Sources* **2005**, *146*, 427.

[15] C.-C. Su, M. He, R. Amine, T. Rojas, L. Cheng, A. T. Ngo, K. Amine, *Energy Environ. Sci.* **2019**, *12*, 1249.
[16] a) X. Chen, X. Shen, B. Li, H.-J. Peng, X.-B. Cheng, B.-Q. Li, X.-Q. Zhang, J.-Q. Huang, Q. Zhang, *Angew. Chem. Int. Ed.* **2018**, *57*, 734; *Angew. Chem.* **2018**, *130*, 742; b) X. Chen, H.-R. Li, X. Shen, Q. Zhang, *Angew. Chem. Int. Ed.* **2018**, *57*, 16643; *Angew. Chem.* **2018**, *130*, 16885.
[17] D. A. Dougherty, E. V. Anslyn, *Modern physical organic chemistry*, University Science Books, Mill Valley, **2006**.
[18] J. Ming, Z. Cao, Y. Wu, W. Wahyudi, W. Wang, X. Guo, L. Cavallo, J.-Y. Hwang, A. Shamim, L.-J. Li, Y.-K. Sun, H. N. Alshareef, *ACS Energy Lett.* **2019**, *4*, 2613.
[19] a) S.-J. Tan, J. Yue, X.-C. Hu, Z.-Z. Shen, W.-P. Wang, J.-Y. Li, T.-T. Zuo, H. Duan, Y. Xiao, Y.-X. Yin, R. Wen, Y.-G. Guo, *Angew. Chem. Int. Ed.* **2019**, *58*, 7802; *Angew. Chem.* **2019**, *131*, 7884; b) J. Wang, Y. Yamada, K. Sodeyama, C. H. Chiang, Y. Tateyama, A. Yamada, *Nat. Commun.* **2016**, *7*, 12032.
[20] F. Cataldo, *Eur. Chem. Bull.* **2015**, *4*, 92.
[21] a) H. Chu, J. Jung, H. Noh, S. Yuk, J. Lee, J.-H. Lee, J. Baek, Y. Roh, H. Kwon, D. Choi, K. Sohn, Y. Kim, H.-T. Kim, *Adv. Energy Mater.* **2020**, *10*, 2000493; b) M. Schmeisser, P. Illner, R. Puchta, A. Zahl, R. van Eldik, *Chem. Eur. J.* **2012**, *18*, 10969.
[22] a) T. T. Hagos, W.-N. Su, C.-J. Huang, B. Thirumalraj, S.-F. Chiu, L. H. Abrha, T. M. Hagos, H. K. Bezabh, G. B. Berhe, W. A. Tegegne, J.-Y. Cherng, Y.-W. Yang, B.-J. Hwang, *J. Power Sources* **2020**, *461*, 228053; b) J. Chen, H. Yang, X. Zhang, J. Lei, H. Zhang, H. Yuan, J. Yang, Y. Nuli, J. Wang, *ACS Appl. Mater. Interfaces* **2019**, *11*, 33419-33427; c) S. Chen, J. Zheng, L. Yu, X. Ren, M. H. Engelhard, C. Niu, H. Lee, W. Xu, J. Xiao, J. Liu, J.-G. Zhang, *Joule* **2018**, *2*, 1548.
[23] C. Y. Go, S. Lim, J. Lee, K. C. Kim, *Energy Storage Mater.* **2021**, *35*, 610.
[24] J. Xiao, Q. Li, Y. Bi, M. Cai, B. Dunn, T. Glossmann, J. Liu, T. Osaka, R. Sugiura, B. Wu, J. Yang, J.-G. Zhang, M. S. Whittingham, *Nat. Energy* **2020**, *5*, 561.
[25] Y. Yang, D. M. Davies, Y. Yin, O. Borodin, J. Z. Lee, C. Fang, M. Olguin, Y. Zhang, E. S. Sablina, X. Wang, C. S. Rustomji, Y. S. Meng, *Joule* **2019**, *3*, 1986.
[26] X. Zhang, Y. Yang, Z. Zhou, *Chem. Soc. Rev.* **2020**, *49*, 3040.
[27] D. Aurbach, E. Zinigrad, Y. Cohen, H. Teller, *Solid State Ionics* **2002**, *148*, 405.
[28] Y. Wu, S.-H. Bo, Y. Xia, *J. Power Sources* **2020**, *467*, 228292.
[29] a) K. Leung, F. Soto, K. Hankins, P. B. Balbuena, K. L. Harrison, *J. Phys. Chem. C* **2016**, *120*, 6302; b) B. Han, Z. Zhang, Y. Zou, K. Xu, G. Xu, H. Wang, H. Meng, Y. Deng, J. Li, M. Gu, *Adv. Mater.* **2021**, *33*, 2100404.
[30] X. Wang, M. Zhang, J. Alvarado, S. Wang, M. Sina, B. Lu, J. Bouwer, W. Xu, J. Xiao, J.-G. Zhang, J. Liu, Y. S. Meng, *Nano Lett.* **2017**, *17*, 7606.
[31] a) W. Zhang, Z. Shen, S. Li, L. Fan, X. Wang, F. Chen, X. Zang, T. Wu, F. Ma, Y. Lu, *Adv. Funct. Mater.* **2020**, *30*, 2003800; b) W. Zhang, Q. Wu, J. Huang, L. Fan, Z. Shen, Y. He, Q. Feng, G. Zhu, Y. Lu, *Adv. Mater.* **2020**, *32*, 2001740.
[32] a) Q. Shi, Y. Zhong, M. Wu, H. Wang, H. Wang, *Proc. Natl. Acad. Sci. USA* **2018**, *115*, 5676; b) Q. Wang, Z. Yao, C. Zhao, T. Verhallen, D. P. Tabor, M. Liu, F. Ooms, F. Kang, A. Aspuru-Guzik, Y.-S. Hu, M. Wagemaker, B. Li, *Nat. Commun.* **2020**, *11*, 4188; c) S. Zhang, G. Yang, Z. Liu, X. Li, X. Wang, R. Chen, F. Wu, Z. Wang, L. Chen, *Nano Lett.* **2021**, *21*, 3310; d) Z. L. Brown, S. Heiskanen, B. L. Lucht, *J. Electrochem. Soc.* **2019**, *166*, A2523; e) S. Liu, X. Ji, N. Piao, J. Chen, N. Eidson, J. Xu, P. Wang, L. Chen, J. Zhang, T. Deng, S. Hou, T. Jin, H. Wan, J. Li, J. Tu, C. Wang, *Angew. Chem. Int. Ed.* **2021**, *60*, 3661; *Angew. Chem.* **2021**, *133*, 3705; f) H. Zhang, G. G. Eshetu, X. Judez, C. Li, L. M. Rodriguez-Martínez, M. Armand, *Angew. Chem. Int. Ed.* **2018**, *57*, 15002; *Angew. Chem.* **2018**, *130*, 15220; g) X.-Q. Zhang, X. Chen, L.-P. Hou, B.-Q. Li, X.-B. Cheng, J.-Q. Huang, Q. Zhang, *ACS Energy Lett.* **2019**, *4*, 411.
[33] C. Fang, J. Li, M. Zhang, Y. Zhang, F. Yang, J. Z. Lee, M.-H. Lee, J. Alvarado, M. A. Schroeder, Y. Yang, B. Lu, N. Williams, M. Ceja, L. Yang, M. Cai, J. Gu, K. Xu, X. Wang, Y. S. Meng, *Nature* **2019**, *572*, 511.
[34] a) X. Cao, X. Ren, L. Zou, M. H. Engelhard, W. Huang, H. Wang, B. E. Matthews, H. Lee, C. Niu, B. W. Arey, Y. Cui, C. Wang, J. Xiao, J. Liu, W. Xu, J.-G. Zhang, *Nat. Energy* **2019**, *4*, 796–805; b) X. Fan, Y. Liu, X. Ou, J. Zhang, B. Zhang, D. Wang, G. Hu, *Chem. Eng. J.* **2020**, *393*, 124709.

Manuscript received: May 6, 2022
Version of record online: September 5, 2022